UCLA
UCLA Previously Published Works

Title
Controlled nanocrystallinity in Gd nanobowls leads to magnetization of 226 emu/g

Permalink
https://escholarship.org/uc/item/7cq3x5z1

Journal
Journal of Applied Physics, 121(9)

ISSN
0021-8979

Authors
Ertas, YN
Bouchard, L-S

Publication Date
2017-03-07

DOI
10.1063/1.4977511

Peer reviewed

Controlled Nanocrystallinity in Gd Nanobowls Leads to Magnetization of 226 emu/g

Y. N. Ertas[1] and L. -S. Bouchard[1,2,3,a]

[1] *Department of Bioengineering, University of California – Los Angeles, 420 Westwood Plaza, Los Angeles, California 90095, USA*

[2] *Department of Chemistry and Biochemistry, University of California – Los Angeles, 607 Charles E. Young Drive East, Los Angeles, California 90095, USA*

[3] *California NanoSystems Institute – UCLA, 570 Westwood Plaza, Los Angeles, California 90095, USA*

[a] Electronic mail: bouchard@chem.ucla.edu

Abstract

Gadolinium (Gd) metal is of great interest in applications such as contrast-enhanced MRI and magnetic cooling. However, it is generally difficult to produce oxide-free and highly magnetic Gd nanoparticles due to the aggressively reactive nature of Gd with oxygen. Herein we utilized a nanofabrication route and optimization of experimental conditions to produce highly magnetic air-stable oxide-free Gd nanoparticles. The nanobowls displayed the highest saturation magnetization to date for Gd, reaching 226.4 emu/g at 2 K. The crystalline composition of Gd is found to affect the observed magnetization values: the higher magnetization is observed for nanoparticles that have a lower content of paramagnetic face-centered cubic (fcc) phase and greater content of ferromagnetic hexagonal close-packed (hcp) phase. The relative fcc content was found to depend on the deposition rate of Gd metal during the nanofabrication process, thereby correlating with altered magnetization.

I. INTRODUCTION

Due to its unique high magnetic moment (268 emu/g at cryogenic temperatures) and high Curie

temperature (293 K) Gd metal has been the subject of considerable interest over the past decade.[1]

The magnetism of Gd arises from the presence of seven unpaired $4f$ electrons and

magnetocrystalline anisotropy.[2] The magnetic properties of Gd display different characteristics

than the standard ferromagnetic $3d$ metals such as Fe and Co.[2] Contrary to non-localized spins

in $3d$ metals, $4f$ spins are indirectly coupled via the Ruderman-Kittel-Kasuya-Yosida interaction

and strongly localized,[3] which brings unique magnetic behavior to Gd at the nanoscale. In recent

years Gd nanoparticles have found uses in magnetocaloric refrigeration,[4] neutron-capture

therapy,[5] temperature sensing[6] and MRI.[7] Previous studies investigated the fabrication and

characterization of thin films,[8] multilayers[9] and nanostructures[10-13] of Gd. In more recent work,[7]

oxide-free Gd nanoparticles have been developed. Up until this work, the primary chemical

synthesis methods for Gd resulted in the formation of oxides due to the aggressively reactive

nature of Gd towards oxygen in ambient air. The applications and uses of Gd have thus been

drastically hampered, thereby limiting our ability to probe the physical and material properties of

Gd in nanoparticle form. The magnetization of Gd thin films is notably different than that of

bulk crystals due to the granular structure, size and shape-related effects.[1] Nanoparticles of Gd

are also expected to possess different magnetic properties than thin.[14] Therefore, there is a need

to produce oxide-free Gd nanoparticles and study their physical properties in nanoparticle form.

Several techniques[13,15-18] have been developed and applied to obtain nanoparticles and nanoscale

powders of Gd, including alkalide reduction, gas-phase, arc-discharge as well as the use of

multilayer precursors. Such nanoparticles were not stable in ambient air, resulting in oxides of

Gd. However, oxides of Gd possess inferior magnetic properties, making them unsuitable for studies of Gd in nanoparticle form.[19] We have recently proposed a novel approach based on a nanofabrication process to produce oxide-free stable Gd nanoparticles whereby a core-shell Gd nanoparticle structure is obtained.[7] The Gd core is grown by deposition of Gd metal under high vacuum conditions whereas the shell layer provides the appropriate capping of the core, preventing oxidation. While this process managed to achieve the highest magnetizations for Gd nanoparticles to date, further optimization of the experimental conditions are possible.

To put our work in context, Table I compares the magnetization of our nanobowls to those of other Gd nanostructures and thin films previously published in the literature. The first general observation is that nanoparticles of Gd generally yield low magnetization values, whereas thin films are closer to bulk values. This is likely a consequence of greater surface effects in nanoparticles. Our nanoparticles exhibit magnetization values that are much closer to the bulk value of Gd compared to other nanoparticle synthesis methods. This is likely due to the oxide-free nature of our fabrication process.[7] In a previous study, it has been claimed that chemical synthesis could achieve oxide-free Gd nanoparticles.[21] However, these nanoparticles may not be exactly oxide-free, as evidenced by the larger magnetizations obtained here via our nanofabrication approach. When constructing this table, we have converted reported magnetization values to emu/g units to enable direct comparison, using the textbook density value of 7.90 g/cm^3 for gadolinium and the unit conversion factor $1\ T = 4\pi.10^{-4}$ emu/cm^3.

TABLE I. Comparison of magnetization values for Gd nanostructures and thin films obtained in previous studies.

Reference #	Type of Gd structure	Magnetization, as reported	Magnetization* in emu/g
This study	Nanoparticle	226.4 emu/g	226.4 emu/g
[1]	Thin film	2.6 T	261.9 emu/g
[9]	Thin film	1,900 emu/cm^3	240.5 emu/g
[19]	Nanorod	460 emu/cm^3	58.2 emu/g
[20]	Bulk	268.4 emu/g	268.4 emu/g
[21]	Nanoparticle	156 emu/g	156 emu/g
[27]	Thin film	640 emu/cm^3	81 emu/g

The main conclusion of this study is the report of the highest saturation magnetization (226.4 emu/g at 2 K) for Gd nanoparticles observed to date. This was obtained through the selection of deposition rate during the nanofabrication process. The deposition rate of the Gd metal resulted in different relative composition of fcc to hcp phases within the construct. This, in turn, correlated with the magnetic properties. Deposition rate during e-beam evaporation may offer a control parameter for nanoparticle properties.

II. EXPERIMENTAL

The nanoparticles were prepared using a nanolithography fabrication process whereby monolayers of polystyrene nanospheres are used as templating pattern for material deposition. Two-inch p-type <100> silicon wafers were spin-coated with a monolayer of polystyrene nanobeads of 200 nm diameter (PS200NM Magsphere Inc., CA). The nanosphere solution was diluted with 1:1 (v/v) methanol solution to facilitate the spreading of the nanospheres on the wafer substrates for a more uniform coating and higher surface coverage. Wafers were also treated by O_2 plasma for 1 min. with a plasma power of 100 W and O_2 flow of 50 sccm before the nanobead coating step to render the wafer surface hydrophilic, enabling the nanosphere solution to better disperse on the surface. Untreated wafers were found to have limited nanobead

4

coverage with multilayer regions after the coating process. Oxygen reactive ion etching (RIE) was performed to reduce the size of the polymer nanospheres. By adjusting the duration and/or plasma power of this step, specific nanosphere sizes could be achieved. However, prolonged etching should be avoided as it eventually results in a loss of spherical shape. Process parameters were adjusted to obtain ~100 nm size spheres with proper spherical shapes, as verified by scanning electron microscopy (SEM). Layers of 10 nm of SiO_2, 10 nm of Gd of 99.95 % purity, and 20 nm of SiO_2 layers were respectively deposited by electron-beam evaporation onto the 15° tilted substrates under high vacuum ($< 10^{-6}$ mtorr) to create Gd@SiO_2 layers onto the etched nanospheres. During the coating process, the wafer holder was rotated continuously at 30 rpm to ensure layer uniformity. Deposition rates and film thickness were controlled in real time using quartz crystal monitoring. Transmission electron microscopy (TEM) was used to confirm the film thicknesses. Prior to deposition of the Gd layer, oxygen content in the vacuum chamber was minimized by pre-depositing the Gd metal while keeping the shutter closed. This further decreases the pressure by absorbing the residual oxygen molecules in the vacuum chamber. Following the deposition of silica and Gd metal layers, the wafer substrates were sonicated in a toluene suspension to etch away the polymer beads, leaving the Gd@SiO_2 nanostructures freely suspended in solution. The nanostructures were then collected by multiple centrifugation steps and suspended in ethanol for future use.

The morphology of the nanostructures was imaged using SEM (JEOL JSM 7500F) and TEM (FEI CM120). High-resolution TEM (HRTEM, FEI Titan S/TEM) operated at 300 kV was used to image the nanolayer compositions. The crystal structures were characterized from powder samples using an X-ray diffractometer (XRD, Bruker D8 Discover Powder X-ray

Diffractometer). The HRTEM samples were prepared using a FEI Nova 600 dual-beam

SEM/FIB (scanning electron microscope/focused ion beam) system. Magnetic property

measurements were conducted using a Quantum Design MPMS® XL superconducting quantum

interference device (SQuID) magnetometer with applied field strengths of up to $\mu_0H = 5$ T.

Magnetization measurements at 5 T are referred to as "saturation magnetization" in this paper

because although Gd is still not completely saturated at 5 T, previous studies showed that further

increases in the applied magnetic field does not lead to a significant increase in the

magnetization for the commonly available laboratory field strengths. The magnetization data

were corrected for the diamagnetic response of the sample holder and other background
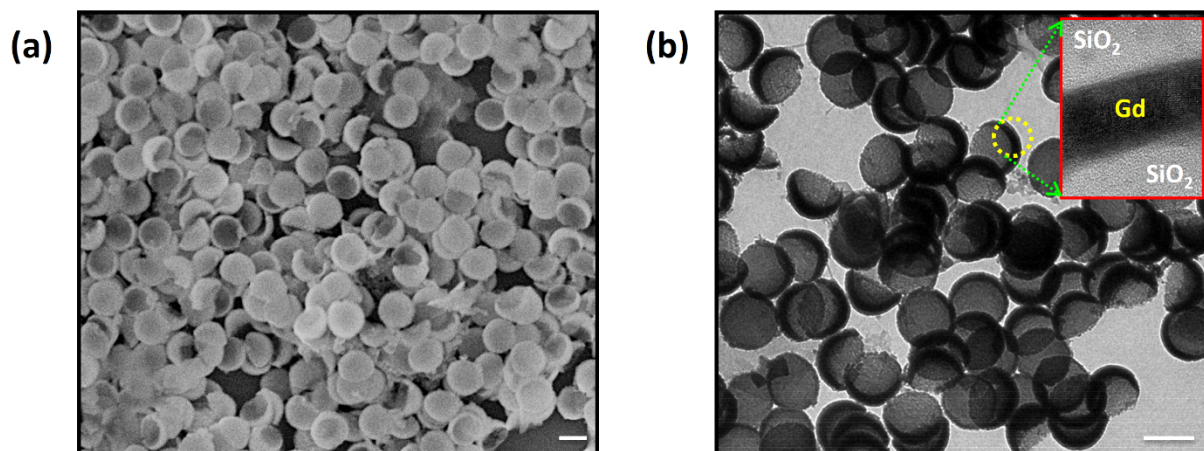
contributions.

III. RESULTS AND DISCUSSION

Figure 1. a) SEM and b) TEM images of the nanobowls. Scale bars, 100 nm. The inset image in

(b) shows the Gd core and silica shell layers as obtained from HRTEM measurements.

Figure 1(a) shows an SEM image of the nanoparticles depicting their bowl-shaped structures. The TEM image in Figure 1(b) reveals the core-shell type structure of the particles where the light gray layer corresponds to the capping SiO_2 layer and the darker shades represent the Gd layer located in the core of the nanoconstruct (middle layer). The inset in Figure 1(b) shows the Gd and SiO_2 layers. The Gd layer was polycrystalline whereas no crystallinity was observed for the silica layer. Both SEM and TEM images confirmed the narrow size distribution of the nanoparticles, which is a direct consequence of the controllable nanofabrication approach employed here.
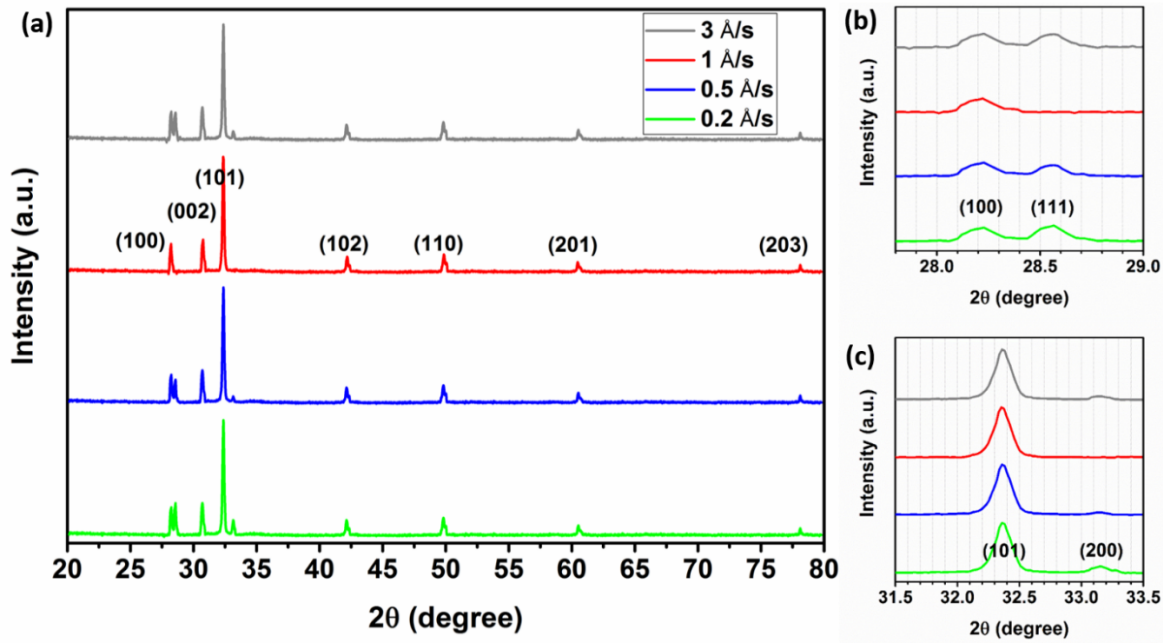

Figure 2. a) XRD spectra of the Gd nanoparticles for varying Gd deposition rates (r) of 0.2 Å/s, 0.5 Å/s, 1 Å/s and 3 Å/s, b) XRD spectra for $27.8° < 2\theta < 29.0°$, c) XRD spectra for $31.5° < 2\theta < 33.5°$

Crystal structure analysis was done at room temperature using Θ–2Θ scans. The shape and width of the XRD spectra peaks were determined using the Rietveld refinement technique. The XRD patterns in Fig. 2(a) reveal that all samples are polycrystalline. A peak analysis reveals the predominance of hcp (hexagonal close-packed) phase of Gd in the samples (JCPDS: 65-0372). A second, smaller, metastable face-centered cubic (fcc), Gd phase (JCPDS: 65-8099) was also observed with $a = (5.35 \pm 0.02)$ Å. Such an fcc phase for Gd was also reported previously[1,12,13,19,22,25,26] for the case of Gd thin films, nanoparticles, and nanostructures. The fcc peaks were observed at $2\theta = 28.6°$ and $2\theta = 33.2°$, referring to (111) and (200) planes, respectively. The highest intensity peak is associated with the hcp (101) orientation at $2\theta = 32.3°$. We also note that there are no detectable reflections originating from oxide or hydride phases, indicating that the Gd nanoparticles are stable as a result of the protective silica shell coating.
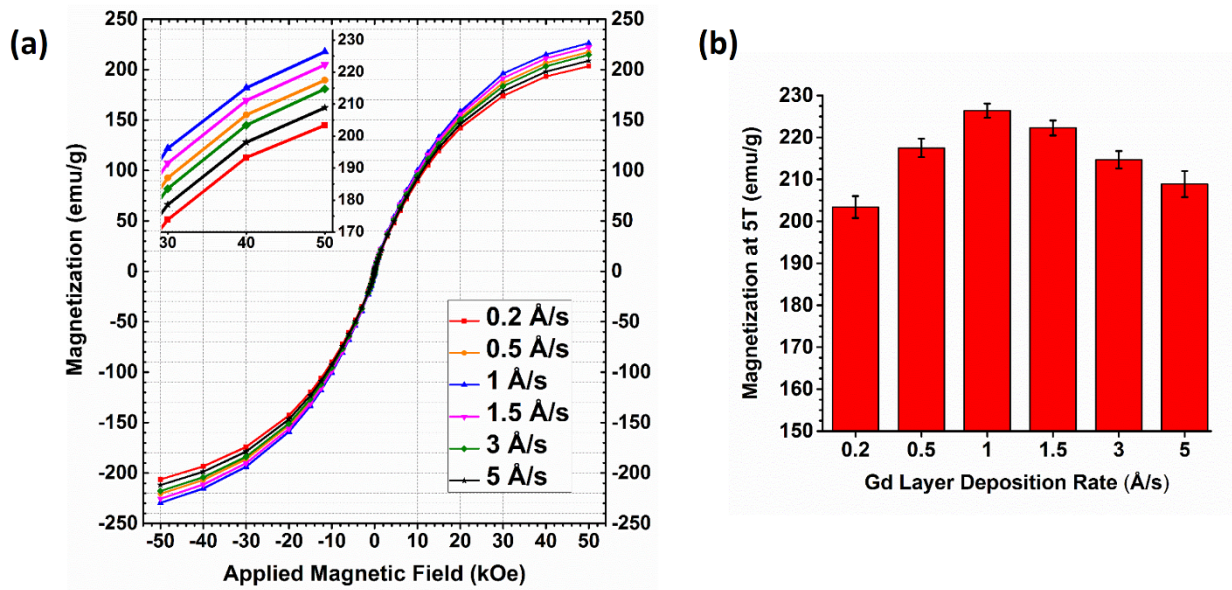

Figure 3. a) Magnetization measurements for different Gd deposition rates. Field-dependent magnetization curves indicate a trend towards saturation in magnetization at high magnetic fields

(5 T). The top left inset shows that saturation magnetization peaks at deposition rate = 1 Å/s, reaching 226.4 emu/g whereas it dips at deposition rate = 0.2 Å/s, decreasing to 203.4 emu/g. The bottom left inset reveals hysteresis associated with ferromagnetism, b) Saturation magnetization versus deposition rate of Gd layer. Error bars indicate the variation of M_s obtained from 5 separate runs for each set of deposition parameters. M_s peaks at 1 Å/s, reaching 226.4 emu/g and decays as the rate goes further on both sides of 1 Å/s.

During the coating process, a deposition rate (r) of r = 0.2 Å/s was used for the Gd layer (green spectrum in Figure 2). This sample contains both hcp and fcc phases. When the Gd deposition rate was increased to r = 0.5 Å/s (blue spectrum), the fcc peak intensities both for (111) and (200) were diminished compared to the r = 0.2 Å/s case (Figures 2b and 2c) whereas the hcp peaks remained unaffected. Therefore, the deposition rate affects the crystallinity of the samples. By controlling the deposition rate, different crystalline compositions could be formed. Scheunert et. al.[25], who studied hcp phase formation in thin films, found up to 2% hcp phase content and identified lattice size distortion and strain as being modulated by the deposition conditions.

Figure 3a shows the magnetization measurements for samples prepared using different Gd deposition rates. For the sample with r = 0.2 Å/s, the saturation magnetization (M_s) was 203.4 emu/g, whereas it jumped up to 217.5 emu/g for r = 0.5 Å/s. The latter is associated with a significantly fcc content (see Figure 2) lower than the r = 0.2 Å/s sample. The majority of earlier reports[12,19,22] on the magnetic properties of the Gd fcc phase found the fcc phase to be paramagnetic compared to the ferromagnetic hcp phase. However, Bertelli et. al. recently reported[27] that a ferromagnetic fcc phase could exist for 10 nm-think Gd thin films buffered with

a Ta layer. Yet, the magnetization of this fcc phase ($\sim$175 emu/cm^3 at 60 K) was found to be lower than that of hcp ($\sim$640 emu/cm^3 at 60 K). This suggests that magnetization in nanoparticles could be increased by growing particles with minimal fcc and maximal hcp content.

To investigate the possibility of optimization, we prepared samples with varying Gd deposition rates of r = 0.2 Å/s, 0.5 Å/s, 1 Å/s, 1.5 Å/s, 3 Å/s and 5 Å/s. As the deposition rate increased from 0.2 Å/s to 1 Å/s, we observed a steady increase in M$_s$. However, this trend is reversed beyond r = 1 Å/s, where M$_s$ begins to decrease, reaching 208.9 emu/g for r = 5 Å/s (Figure 3a). A saturation value of 226.4 emu/g was achieved at r = 1 Å/s which displayed no detectable presence of fcc phase (see XRD measurements, Figures 2a, 2b, 2c). Figure 2b and 2c shows that the (111) and (200) fcc peaks are stronger for r = 0.2 Å/s than they are for r = 3 Å/s, which should result in a higher M$_s$ value for the latter. For these two rates, the M$_s$ values are 203.4 emu/g and 214.7 emu/g, respectively.

The magnetization measurements of Figure 3a were recorded for applied fields in the range -5 T to 5 T. Standard ferromagnetic behavior with hysteresis is observed for all cases even though XRD spectra indicates some fcc contributions are present in most of the samples. The presence of the ferromagnetic hcp phase in all our samples is consistent with the observation of magnetic hysteresis. The presence of a small amount of paramagnetic fcc phase in the samples is reflected in the magnetic measurements as far as its effect is to decrease the saturation magnetization (Figs. 3 and 4). The saturation magnetization of the fcc phase of Gd has been shown to be approximately 4 times less than that of hcp Gd ($\sim$ 175 emu/cm^3 vs. $\sim$ 640 emu/cm^3 at 60 K)

according to Bertelli *et. al.*[27] From the XRD data we compute s, the ratio between the area under the strongest Bragg peaks of the hcp (101) and fcc (200) phases, defined as $s = A_{fcc} / A_{hcp}$ (%). For the sample with lowest magnetization (r = 0.2 Å/s), s was found to be 12.2 %, whereas for the optimal condition (highest M_s, r = 1 Å/s), s approaches zero as the fcc peaks were no longer detectable, buried in the noise. These results are shown in Table I for different deposition rates. We note the inverse correlation between s and M_s. We calculate the expected value of M_s values based on the measured M_s value for fcc Gd (Ref. [24]) as a weighted average of fcc and hcp fractions (1):

$$\text{expected } M_s = (226.4)(1 - s) + \left(\frac{226.4}{4}\right)(s), \tag{1}$$

where s is a number between 0 and 1 (expressed as a percentage in Table II) and $\frac{226.4}{4}$ is the M_s value for fcc Gd from Ref. [27]. The expected values of M_s are close to the observed values (Table II). Thus, we conclude that the observed decreases in saturation magnetization values at different deposition rates can be accounted for by the less magnetic fcc fraction.

TABLE II. Crystalline phase composition and corresponding magnetization values for Gd nanobowls fabricated using different Gd deposition rates.

Gd deposition rate (Å/s)	Area fcc (a.u.)	Area hcp (a.u.)	s factor (%)	Expected M_s (emu/g)	Observed M_s (emu/g)
0.2	57.4	469.1	12.2 %	205.7	203.4
0.5	19.2	468.7	4.1 %	219.4	217.5
1	~ 0	469.4	~ 0 %	226.4	226.4
3	30.8	471.7	6.5 %	215.4	214.7

To check that the observed changes in M_s are not due to random errors or other effects, error bars were obtained by repeating the experiments on different days using the same nominal parameters. Figure 3b shows the saturation magnetization values for different Gd deposition rates and the corresponding error bars for each case, which represent 5 different measurements. It is seen that the statistical fluctuations in magnetization values (for example, $M_s = 226.4 \pm 1.7$ emu/g for r = 1 Å/s) are lower than the observed changes in M_s. Thus, random errors do not account for the observed trends in Figure 3b. We conclude that the deposition rate has a direct effect on the observed magnetization values.

The lowest saturation magnetization value was found at the lowest deposition rate (r = 0.2 Å/s), where the highest content of fcc phase was measured. The presence of the fcc phase could lead to a significant contribution of intergrain and intragrain anisotropies.[1] The highest saturation magnetization we obtained was 226.4 emu/g (at 2 K), which is lower than the theoretical maximum (268 emu/g) but higher than any other Gd nanoparticles produced to date. The difference from the bulk value may be due to interfacial effects[22,23] present in nanostructures. There have been several reports[1,25] of Gd thin films preferring to nucleate at a seed boundary in a paramagnetic fcc phase. Since the substrate (curved surface of amorphous silica here) affects the growth, other choices of geometries and materials such as Mn, Pd, Cr or W would be expected to lead to different magnetic properties.[28] The polycrystalline nature[23] of the samples, randomly grain formations,[10,11,18,23,25] crystal defects[11] and stress[18,25,29] likely act as barriers to achieving high magnetism by distorting the magnetization uniformity.

IV. CONCLUSION

In summary, we have applied a nanofabrication approach to prepare air stable core-shell Gd nanoparticles with high magnetic moments. Crystallinity of the nanoparticles played an important role in maximizing magnetization. The ferromagnetic hcp phase of Gd was the main dominant crystal structure whereas small amounts of paramagnetic fcc phase could be detected. We have experimentally shown that lower fcc content leads to higher saturation magnetization. We found that by adjusting the deposition rate of Gd, it is possible to control the amount of fcc content in the lattice. A deposition rate of 1 Å/s led to the highest magnetic moment of 226.4 emu/g for Gd. Such a high magnetization has never been observed experimentally to date for Gd nanoparticles. Stability of the nanoparticles along with their high magnetizations could give rise to new applications for Gd which have not been possible so far due to oxidation problems in ambient air.

References

1. G. Scheunert, W. R. Hendren, C. Ward and R. M. Bowman, Appl. Phys. Lett. **101**, 142407 (2012).

2. M. Chakravorty and A. K. Raychaudhuri, J. Appl. Phys. **115**, 054308 (2014).

3. M. A. Ruderman and C. Kittel, Phys. Rev. **96**, 99 (1954).

4. K. A. Gschneidner, V. K. Pecharsky and A. O. Tsokol, Rep. Prog. Phys. **68**, 1479 (2005).

5. D. C. F. Soares, M. A. de Barros Correia Menezes, R. G. dos Santos and G. A. Ramaldes, J. Radioanal. Nucl. Chem. **284**, 315 (2010).

6. S. M. Borisov and I. Klimant, Anal. Bioanal. Chem. **404**, 2797 (2012).

7. Y. N. Ertas, N. N. Jarenwattananon, and L. S. Bouchard, Chem. Mater. **27**, 5371 (2015).

8. U. Stetter, M. Farle, K. Baberschke and W. G. Clark, Phys. Rev. B **45**, 503 (1992).

9. J. S. Jiang and C. L. Chien, J. Appl. Phys. **79**, 5615 (1996).

10. M. Yue, J. X. Zhang, H. Zeng and K. Wang, Appl. Phys. Lett. **89**, 232504 (2006).

11. F. Döbrich, M. Elmas, A. Ferdinand, J. Markmann, M. Sharp, H. Eckerlebe, J. Kohlbrecher, R. Birringer and A. Michels, J. Phys.: Condens. Matter **21**, 156003 (2009).

12. X. G. Liu, D. Y. Geng, Q. Zhang, J. J. Jiang, W. Liu and Z. D. Zhang, Appl. Phys. Lett. **94**, 103104 (2009).

13. I. Aruna, B. R. Mehta, L. K. Malhotra and S. M. Shivaprasad, Adv. Funct. Mater. **15**, 131 (2005).

14. M. J. O'Shea and P. Perera, J. Appl. Phys. 85, 4322 (1999).

15. J. A. Nelson, L. H. Bennett and M. J. Wagner, J. Am. Chem. Soc. **124**, 2979 (2002).

16. Y. Z. Shao, C. H. Shek and J. K. L. Lai, J. Mater. Res. **13**, 2969 (1998).

17. P. Z. Sil. Škorvánek, J. Kováč, D. Y. Geng, X. G. Zhao and Z. D. Zhang, J. Appl. Phys. **94**, 6779 (2003).

18. , Z. C. Yan, Y. H. Huang, Y. Zhang, H. Okumura, J. Q. Xiao, S. Stoyanov, V. Skumryev, G. C. Hadjipanayis and C. Nelson, Phys. Rev. B: Condens. Matter Mater. Phys. **67**, 054403 (2003).

19. C. J. Hsu, S. V. Prikhodko, C. Y. Wang, L. J. Chen and G. P. Carman, J. Appl. Phys. **111**, 053916 (2012).

20. H. E. Nigh, S. Legwold and F. H. Spedding, Phys. Rev. **132**, 1092 (1963).

21. C. Yan and M. Wagner, Nano Lett. **13**, 2611 (2013).

22. C. Ward, G. Scheunert, W. R. Hendren, R. Hardeman, M. A. Gubbins and R. M. Bowman, Appl. Phys. Lett. **102**, 092403 (2013).

23. S. P. Mathew and S. N. Kaul, J. Phys.: Condens. Matter **24**, 256008 (2012).

24. M. Chakravorty and A. K. Raychaudhuri, J. Appl. Phys. **117**, 034301 (2015).

25. G. Scheunert, C. Ward, W. R. Hendren, A. A. Lapicki, R. Hardeman, M. Mooney, M. Gubbins and R. M. Bowman, Journal of Physics D: Applied Physics **47**, 415005 (2014).

26. A. E. Curzon and H. G. Chlebek, J. Phys. F: Metal Phys. **3**, (1973).

27. T. P. Bertelli, E. C. Passamani, C. Larica1, V. P. Nascimento, A. Y. Takeuchi and M. S. Pessoa, J. Appl. Phys. **117**, 203904 (2015).

28. G. Scheunert, O. Heinonen, R. Hardeman, A. Lapicki, M. Gubbins, and R. M. Bowman, Appl. Phys. Rev. **3**, 011301 (2016).

29. G. Scheunert, W. R. Hendren, C. Ward and R. M. Bowman, Appl. Phys. Lett. **101**, 142407 (2012).